

The 'Green' Ni-UGSO Catalyst for the Hydrogen Production Under Various Reforming Regimes

Mostafa Chamoumi and Nicolas Abatzoglou

Supplementary information

A. Thermodynamics of DRM and SRM reactions

Figure S1 shows the evolutions of the free enthalpies of the $\Delta G(T)$ reactions as a function of temperature for DRM and SRM calculated using the FactSage 7.0 software.

- For the reaction of DRM ($\text{CH}_4 + \text{CO}_2 \rightarrow 2\text{CO} + 2\text{H}_2$), the variation of the free enthalpy with temperature is expressed by the relation: $\Delta G(T)_{\text{DRM}} (\text{kJ} / \text{mol}) = -0.2835T + 259.56$ (Eq.17)
- The free enthalpy variation with temperature for the reaction of the SRM ($\text{CH}_4 + \text{H}_2\text{O} \rightarrow \text{CO} + 3\text{H}_2$) is given below: $\Delta G(T)_{\text{SRM}} (\text{kJ} / \text{mol}) = -0.2517T + 224.3$ (Eq.18)
- The $\Delta G(T)$ measurements indicates that the DRM reaction is possible starting at 916K and that of the SRM at 891K ($\Delta G \leq 0$) and upwards.
- It should be noted that throughout the temperature range studied, DRM and SRM have positive $\Delta H(T)$ enthalpies values. This indicates that such reactions are endothermic: an external supply of heat is therefore necessary.

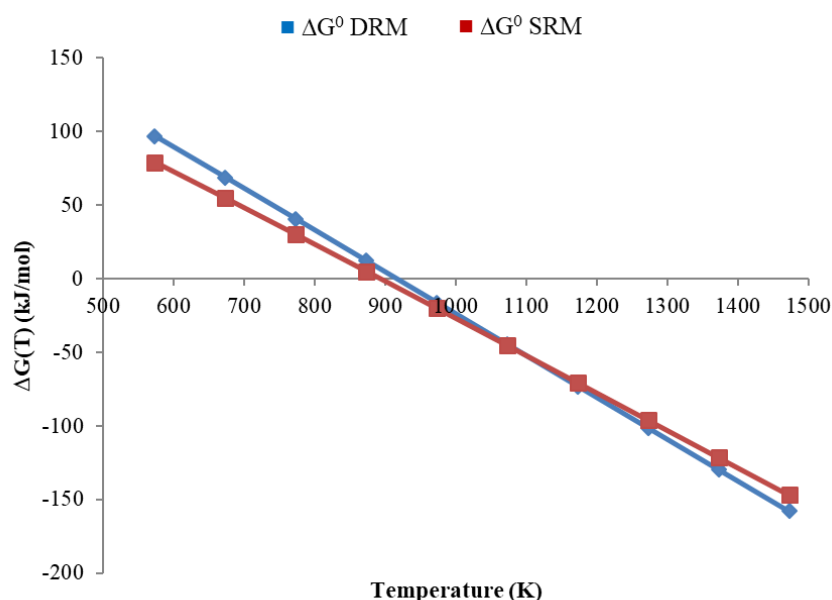


Figure S1. Evolution of free enthalpies ($\Delta G(T)$) of DRM and SRM reactions as a function of temperature

The conversions of CH_4 and CO_2 as well as the compositions of gaseous mixtures (H_2 , CO , H_2O , CH_4 and CO_2) and graphitic carbon C , calculated at thermodynamic equilibrium between 973K and 1273K, are given in Figure S2 for the DRM reaction. Figure S3 shows the evolution of the H_2/CO ratio at thermodynamic equilibrium for DRM. The values indicated correspond to the molar composition of the mixture obtained from one mole of CH_4 and one mole of CO_2 .

At thermodynamic equilibrium, starting at 1123K, the DRM reaction shows a molar ratio of $\text{H}_2/\text{CO} = 1$ and conversion rates of CH_4 and CO_2 of 97% and 95%. However, it is only at or above 1223K that there is no more formation of carbon.

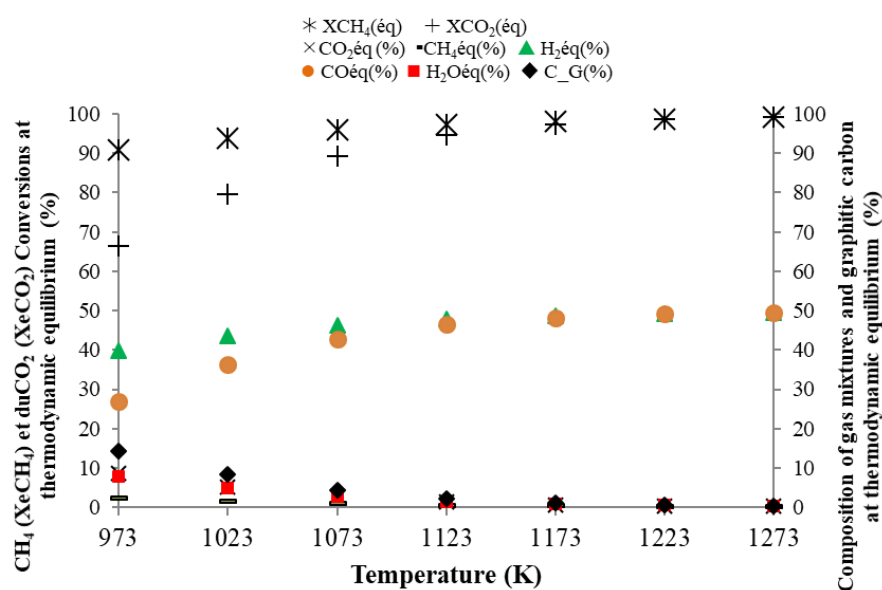


Figure S2. CH_4 and CO_2 conversions and composition of gas mixtures and graphitic carbon at thermodynamic equilibrium for the DRM reaction

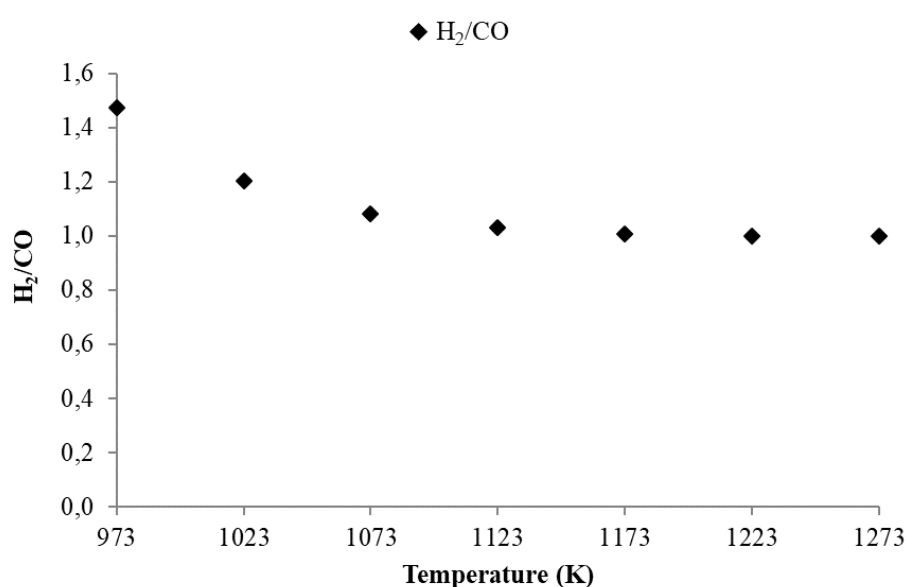


Figure S3. Thermodynamic equilibrium H_2/CO ratio for the DRM reaction

For the SRM reaction, conversion rates of CH_4 and H_2O as well as compositions of gaseous mixtures (H_2 , CO , CO_2 , CH_4 and H_2O) and graphitic carbon C , calculated at thermodynamic

equilibrium between 973K and 1273K, are given in Figure S4. Additionally, Figure S5 shows the evolution of the H_2/CO ratio at thermodynamic equilibrium for the SRM. The values indicated correspond to the molar composition of the mixture obtained from one mole of CH_4 and one mole of H_2O .

At thermodynamic equilibrium, at or above 1123K, the SRM reaction shows a molar ratio of $H_2/CO = 3$ and CH_4 and H_2O conversion rates of 94% and 95% respectively. It should be noted that at or above this temperature (1123K), carbon formation no longer occurs.

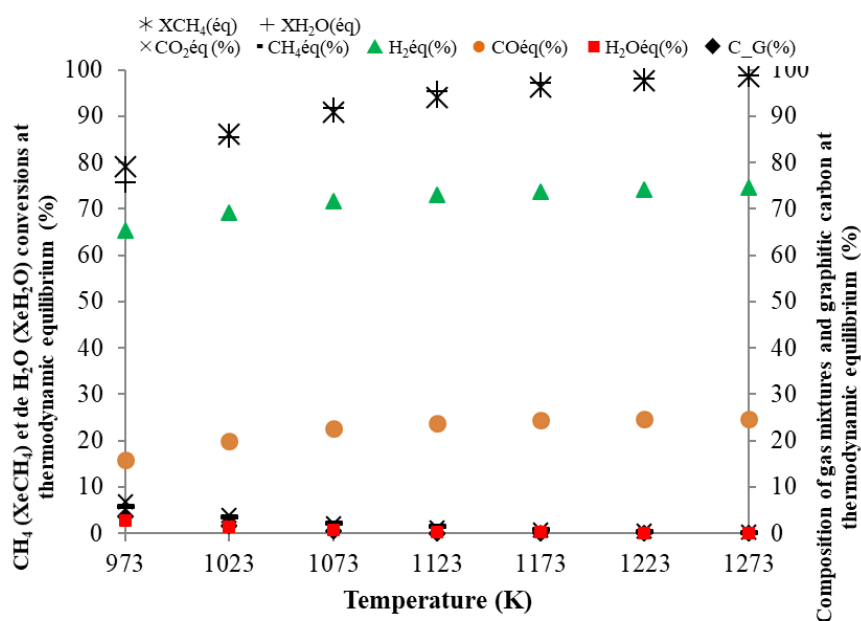


Figure S4. CH_4 and CO_2 conversions and composition of gas mixtures and graphitic carbon at thermodynamic equilibrium for the SRM reaction

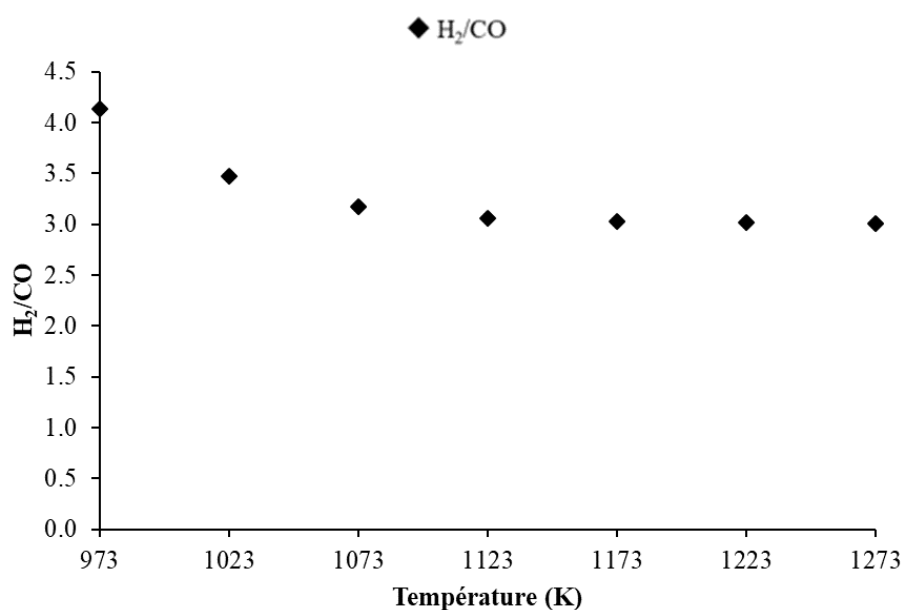


Figure S5. Thermodynamic equilibrium H_2/CO ratio for the SRM reaction

B. Results

Influence of the active phase content on the catalytic activity

Figure S6 shows the evolution of CO₂ conversions and Figure S7 and Figure S8 show the H₂ yield and the H₂/CO ratio, respectively, along the reforming tests.

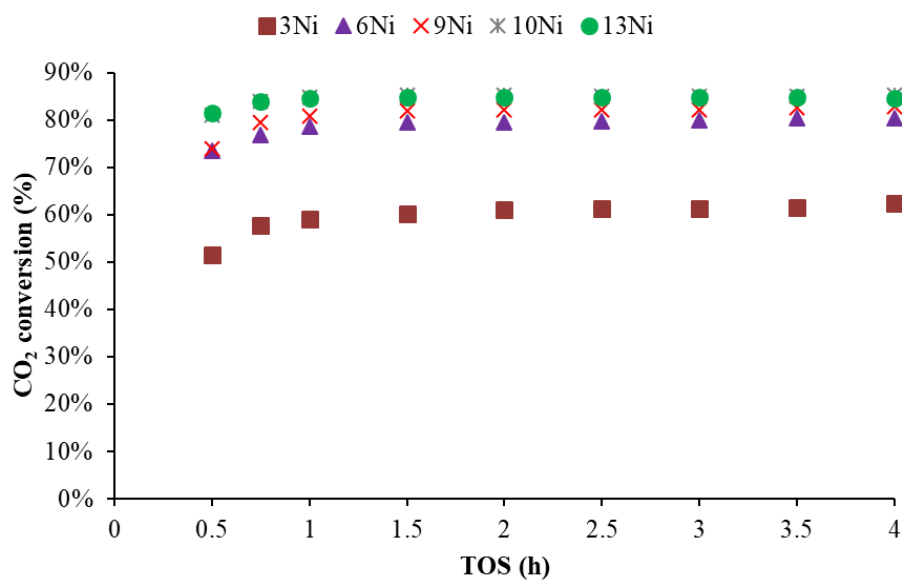


Figure S6. Effect of Ni content: evolution of CO₂ conversion as a function of time at 842°C, CO₂/CH₄=1.25

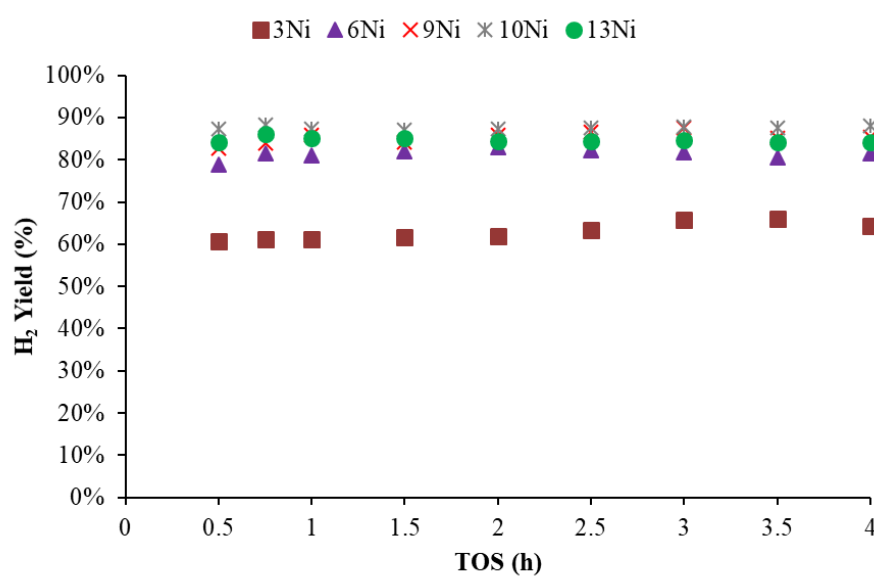


Figure S7. Effect of Ni content: evolution of H₂ yield as a function of time at 842°C, CO₂/CH₄=1.25

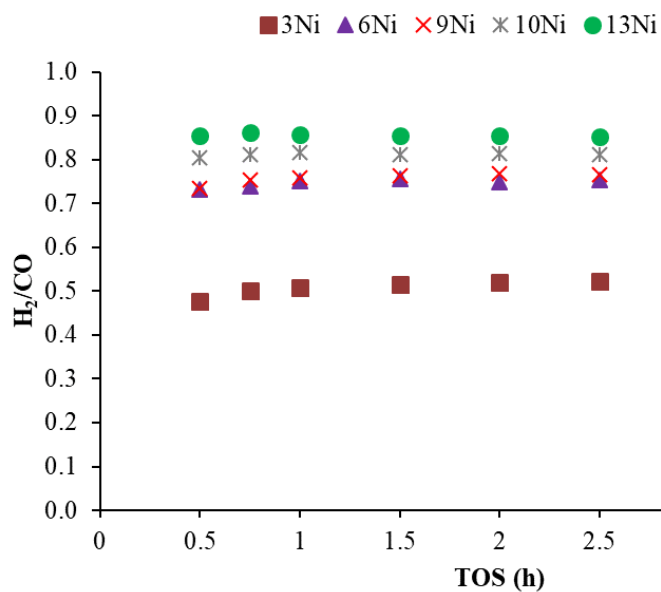
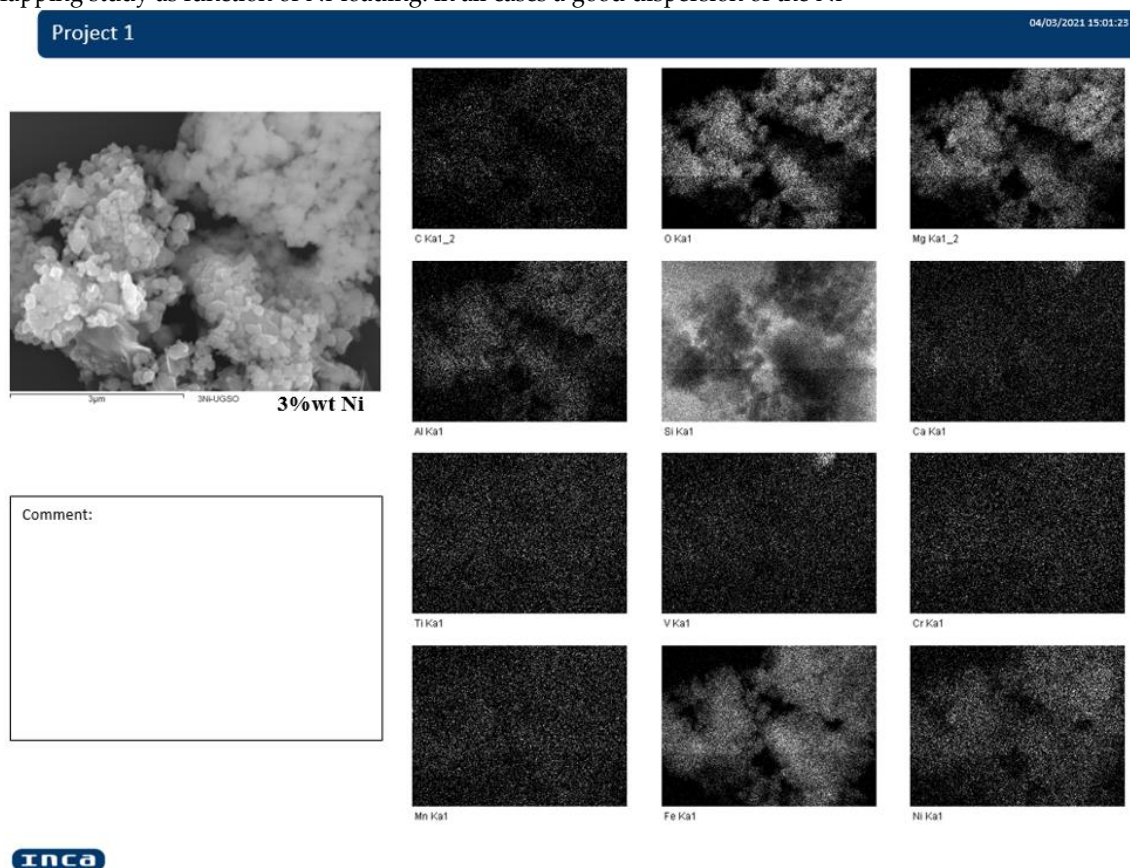
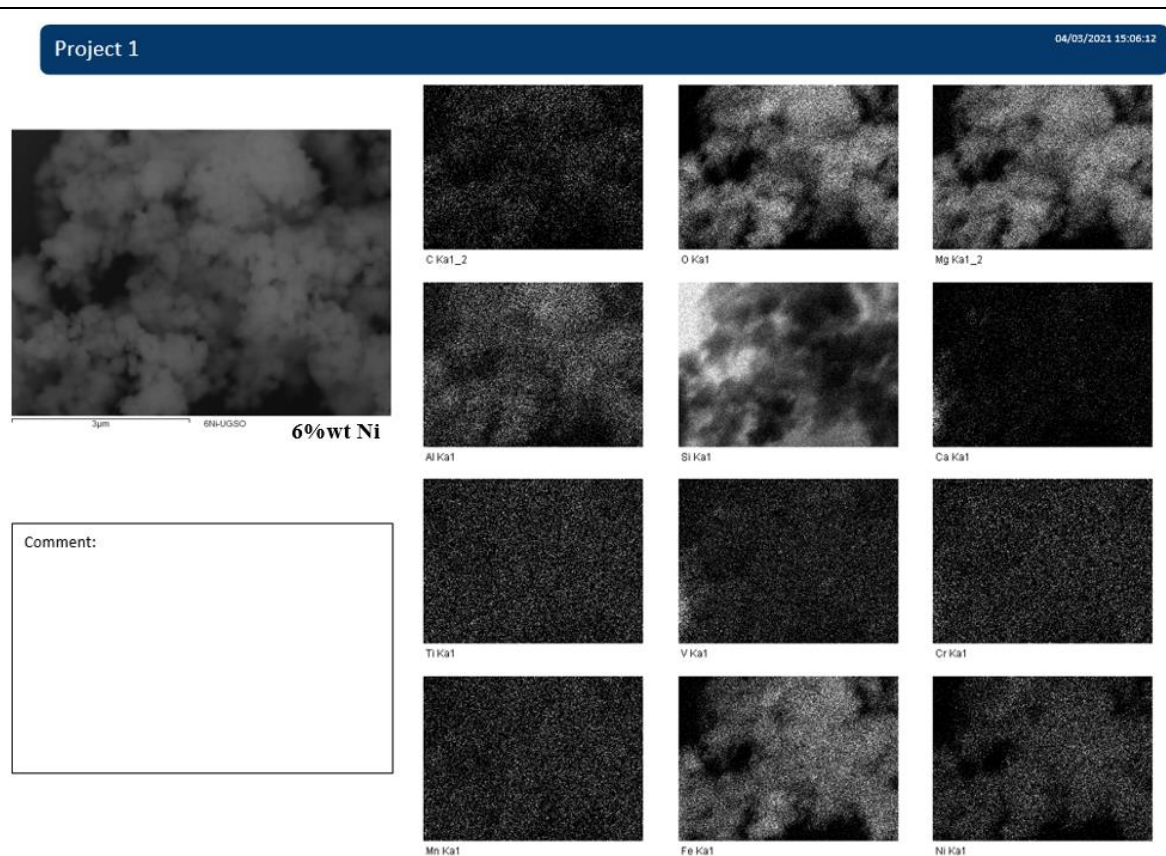
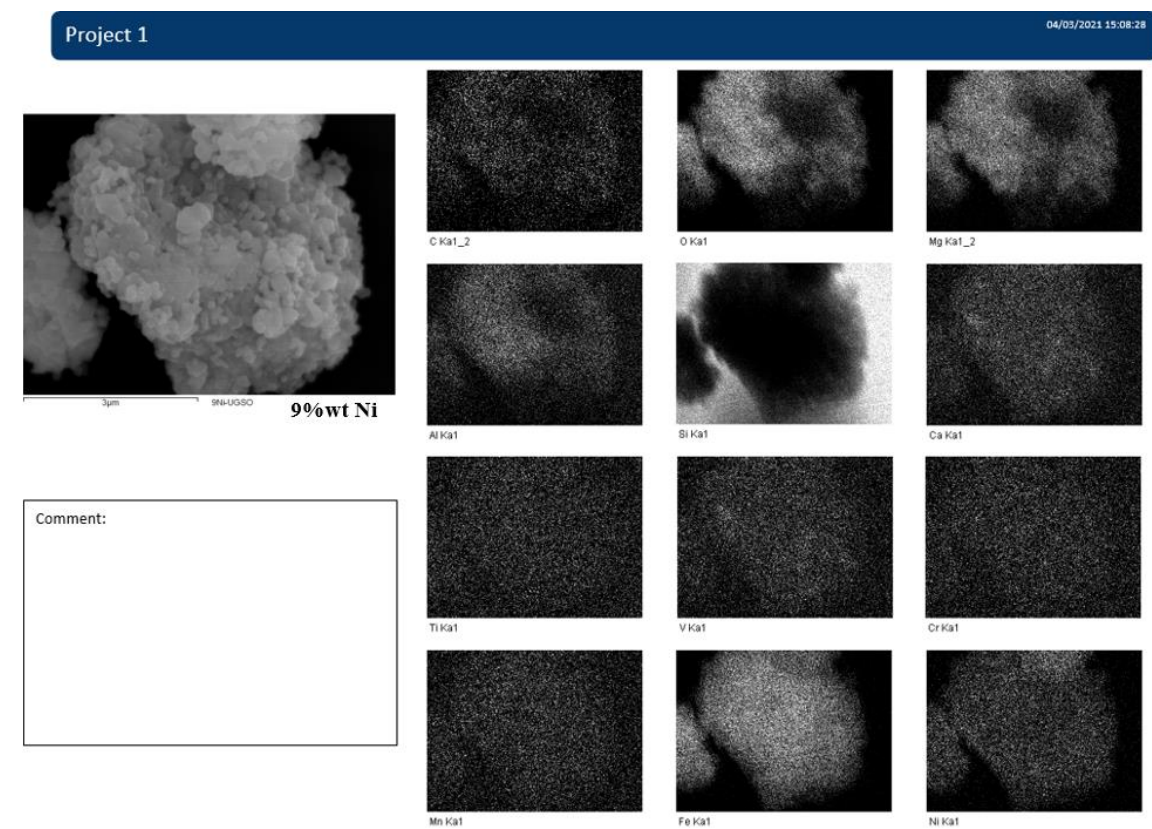
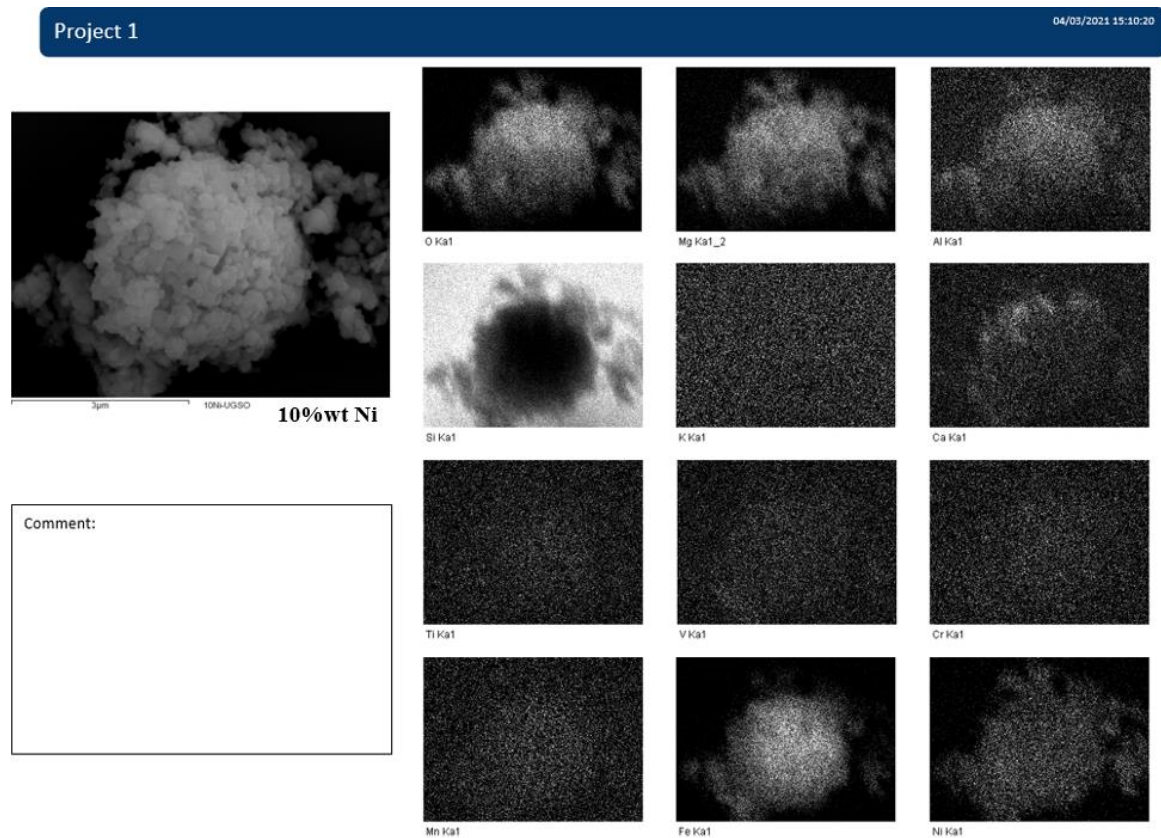
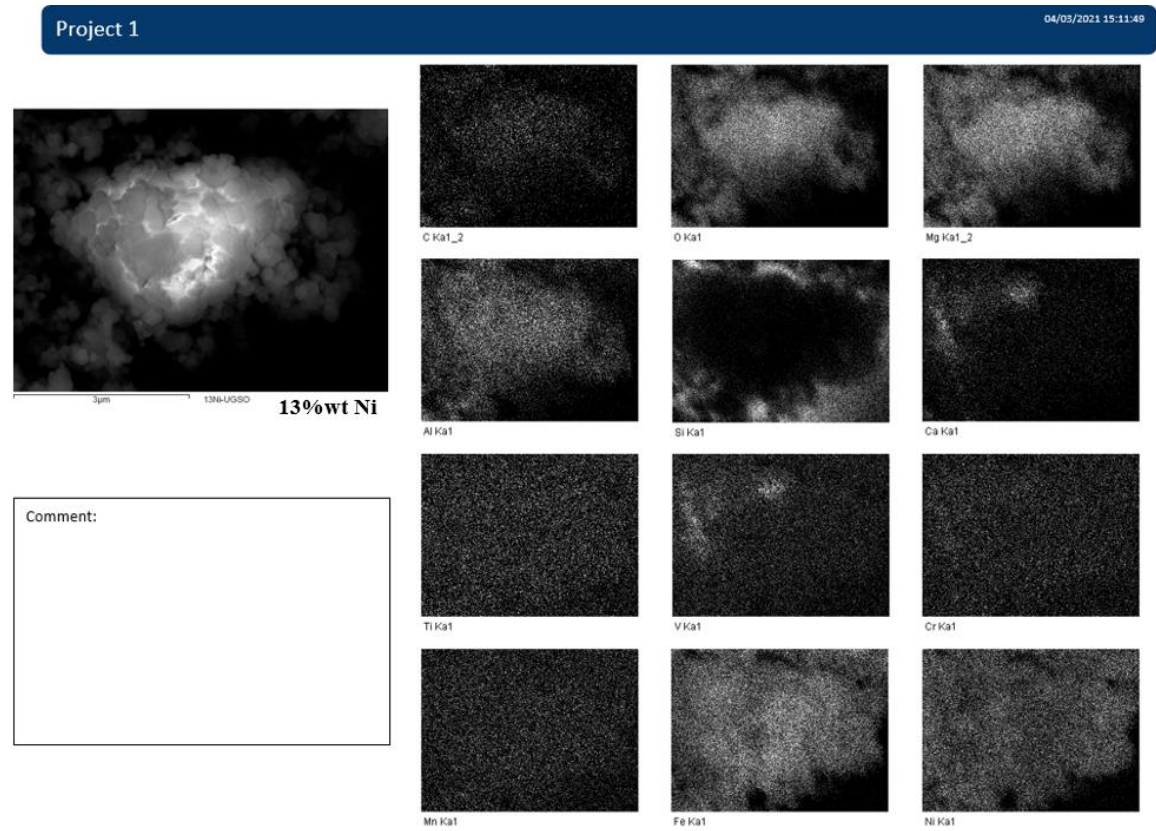


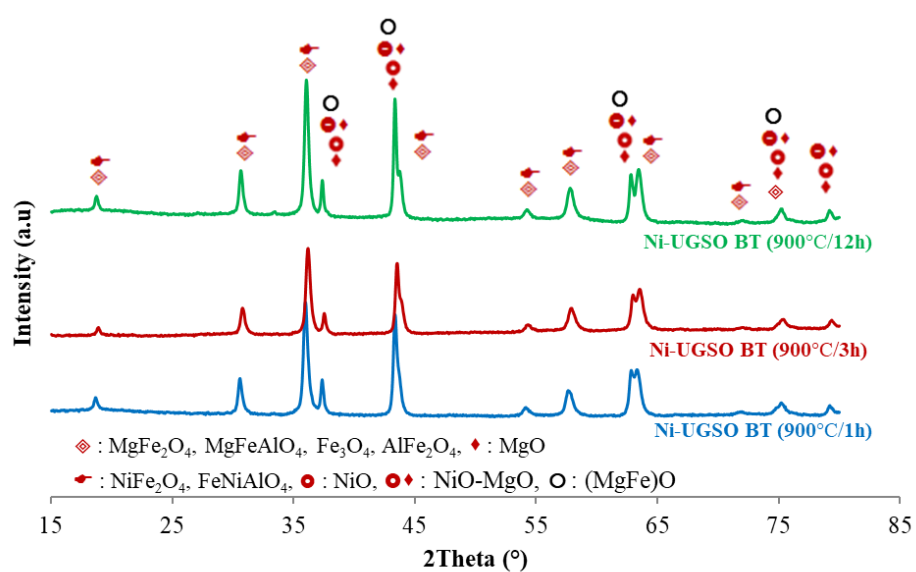
Figure S8. Effect of Ni content: evolution of H_2/CO ratio as a function of time at $842^\circ C$, $CO_2/CH_4=1.25$

Mapping study as function of Ni-loading: in all cases a good dispersion of the Ni



**Inca****Inca**

**Inca****Inca****Figure S9.** Mapping study as function of Ni-loading

Influence of catalyst calcination time**Figure S10.** XRD catalysts calcined at 900°C for 1h, 3h and 12h

Representativeness of UGSO mining residue lots

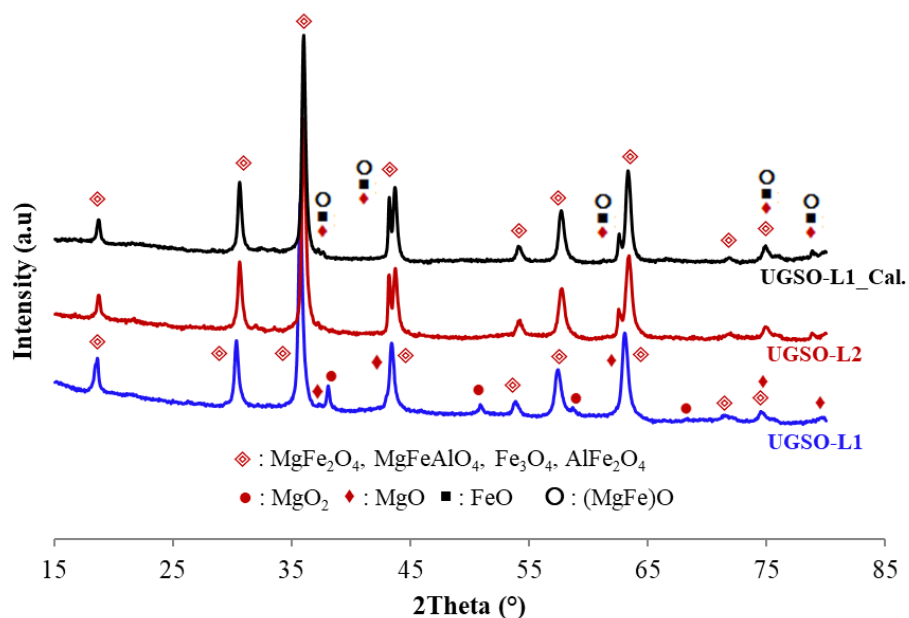


Figure S11. XRD of the two lots of UGSO compared to that of the UGSO L1 calcined at 900°C/12h

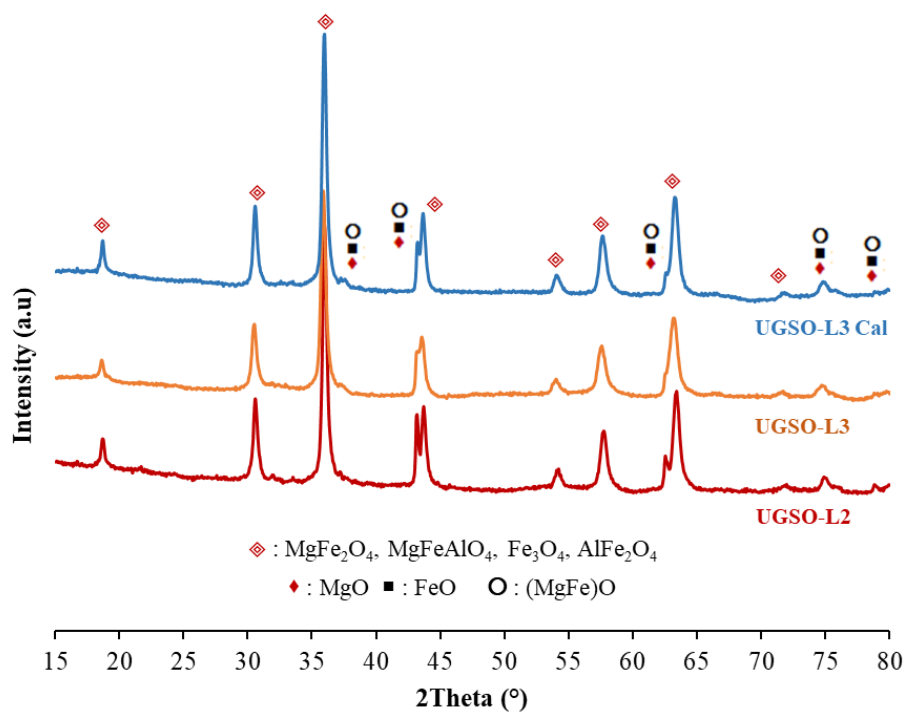


Figure S12. XRD of the of UGSO-L2 compared to that of the UGSO-L3 calcined at 900°C/12h

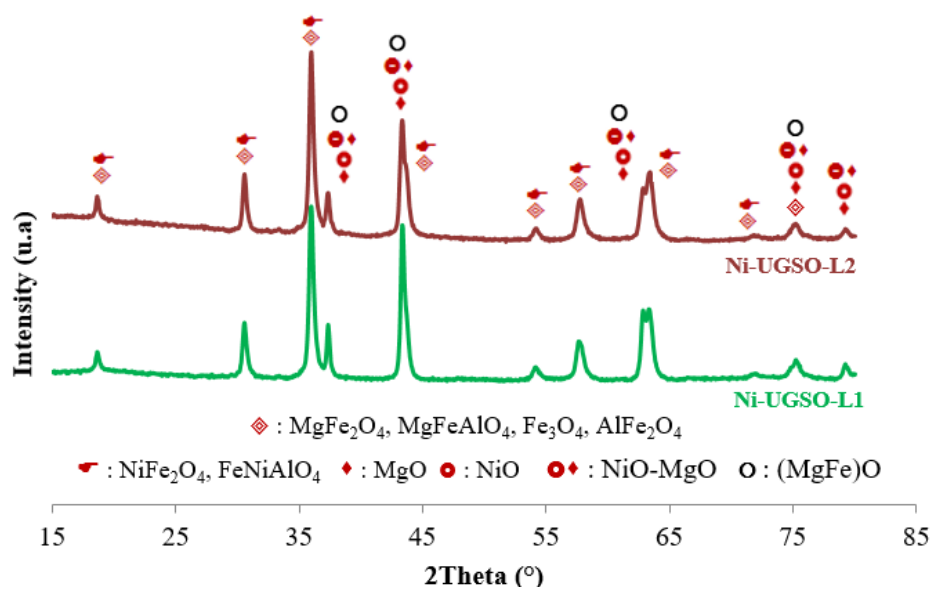


Figure S13. XRD of Ni-UGSO catalysts from 2 lots calcined at 900°C for 1h

Ni-UGSO sulfur poisoning resistance

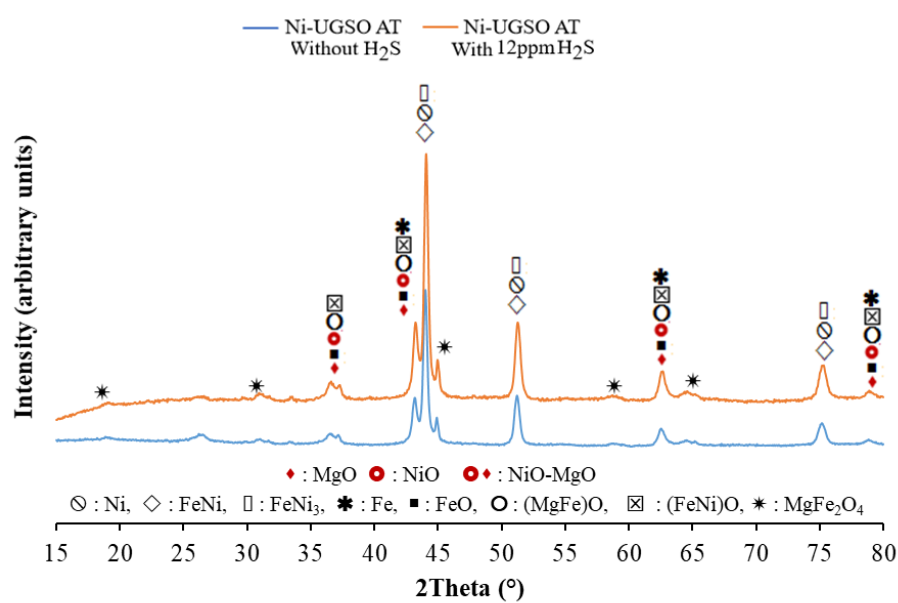


Figure S14. XRD of spent Ni-UGSO catalysts without and with H_2S

Ni-UGSO performance as a catalyst for steam methane reforming (SRM)

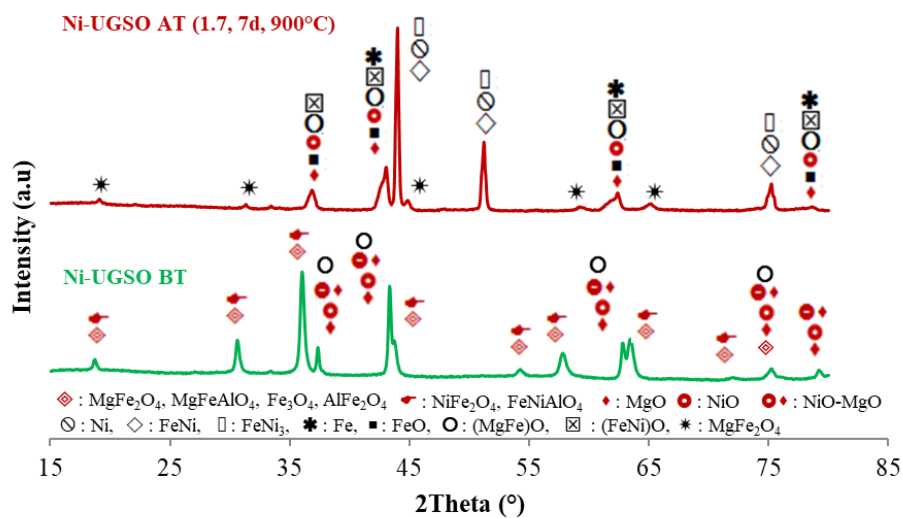


Figure S15. XRD of Ni-UGSO used for 7 days at the SRM ($\text{H}_2\text{O}/\text{CH}_4=1.7$, 900°C) compared to the fresh catalyst Ni-UGSO BT

Ni-UGSO performance as a catalyst for mixed methane dry and steam reforming

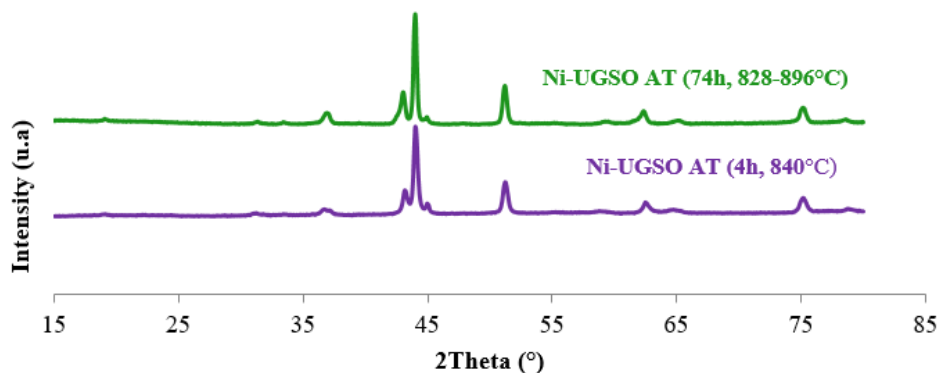


Figure S16. XRD of used catalyst Ni-UGSO AT (4h & 74h) ($\text{CO}_2/\text{CH}_4 = 0.97$ and $\text{H}_2\text{O}/\text{CH}_4 = 0.15$)

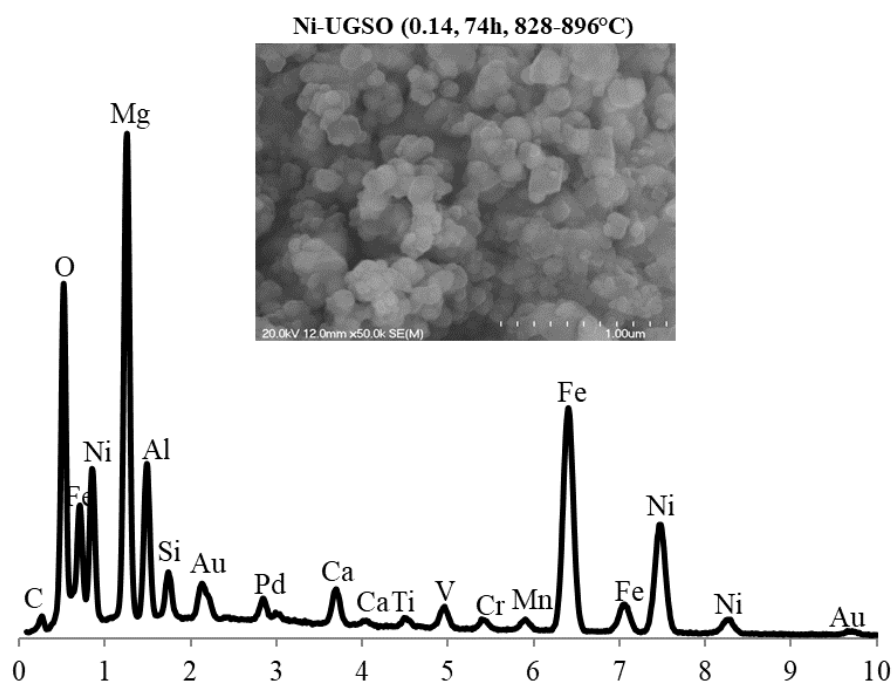


Figure S17. SEM-EDX of used catalyst Ni-UGSO AT (4h & 74h) ($\text{CO}_2/\text{CH}_4 = 0.97$ and $\text{H}_2\text{O}/\text{CH}_4 = 0.15$)